ACS Catalysis

Research Article

pubs.acs.org/acscatalysis

Mesoporous Beta Zeolite-Supported Ruthenium Nanoparticles for Selective Conversion of Synthesis Gas to C_5–C_{11} Isoparaffins

Kang Cheng,[†] Jincan Kang,[†,‡] Shuiwang Huang,[†] Zhenya You,[†] Qinghong Zhang,*[,†] Jiansheng Ding,[‡] Weiqi Hua,[‡] Yinchuan Lou,[‡] Weiping Deng,[†] and Ye Wang*[,†]

[†]State Key Laboratory of Physical Chemistry of Solid Surfaces, National Engineering Laboratory for Green Chemical Productions of Alcohols, Ethers and Esters, College of Chemistry and Chemical Engineering, Xiamen University, Xiamen 361005, China

[‡]Yantai Wanhua Polyurethanes Co., LTD, Yantai 264002, China

ABSTRACT: Mesoporous beta (meso-beta) zeolites prepared by post-treatment of H-beta with NaOH aqueous solution were studied as supports of Ru catalysts for Fischer–Tropsch (FT) synthesis. The size and volume of the mesopores increased with the concentration of NaOH. The Brønsted acidity declined because Na^+ ions were exchanged into the meso-beta during the post-treatment, and a further ion exchange of the meso-beta with NH_4^+ followed by calcination, forming H-meso-beta, could recover the Brønsted acidity. The use of H-meso-beta or meso-beta instead of H-beta or Na-beta as the support for FT synthesis decreased the selectivities to CH_4 and heavier hydrocarbons (C_{12}^+) and increased that to C_5–C_{11} hydrocarbons. The C_5–C_{11} selectivity depended on the concentration of NaOH used for meso-beta preparation. Under an optimum NaOH concentration, a C_5–C_{11} selectivity of 77%, significantly higher than the maximum expected from Anderson–Schulz–Flory distribution (~45%), was attained with a ratio of isoparaffins to *n*-paraffins being 2.7. The mesoporosity and the unique acidity of the meso-beta probably contribute to the selective hydrocracking of the primary heavier hydrocarbons formed on Ru nanoparticles into gasoline-range liquid fuels.

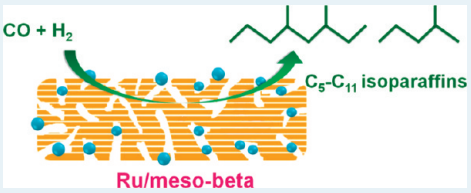

KEYWORDS: *mesoporous zeolite, ruthenium nanoparticles, Fischer–Tropsch synthesis, synthesis gas, gasoline, selectivity control*

1. INTRODUCTION

In recent years, hierarchical zeolites containing both micropores and mesopores have attracted much attention as a new type of promising catalytic materials.[1−10] These materials combine the advantages of the conventional microporous zeolites, which possess acidic catalytic functions and shape-selective features and are stable at high temperatures because of the crystalline structures, and the mesoporous materials with efficient mass transport. Mesoporous zeolites have demonstrated improved performances in several catalytic reactions, particularly the acid-catalyzed reactions. For examples, the activity and selectivity for the alkylation of benzene to ethylbenzene or cumene were increased by using mesoporous ZSM-5 or mesoporous mordenite instead of conventional H-ZSM-5 and mordenite.[11−13] Mesoporous Y or mesoporous ZSM-5 zeolites exhibited improved product distributions or enhanced activity and stability for the hydrocracking of heavy hydrocarbons.[14−16] Mesoporous beta zeolite-supported Pd showed higher catalytic performances in the deep hydrogenation of aromatics.[17] The presence of mesopores in ZSM-5 suppressed the catalyst deactivation in the conversion of methanol to hydrocarbons.[18]

Fischer–Tropsch (FT) synthesis, that is, the conversion of synthesis gas (syngas, CO + H_2) to hydrocarbons, is a crucial step in the indirect transformation of nonpetroleum carbon resources such as natural gas, coal and biomass into fuels such as gasoline and diesel or chemicals such as lower olefins. Because of the global demand for a decreased dependence on petroleum, FT synthesis has received renewed interest in recent years.[19−24]

One of biggest challenges in FT synthesis is selectivity control. Over most conventional FT catalysts, the products follow the Anderson–Schulz–Flory (ASF) distribution, and such a distribution is unselective for the production of middle-distillate products, which are usually the target products.[24] For example, the maximum selectivities to C_5–C_{11} (gasoline-range) and C_{12}–C_{20} (diesel-range) hydrocarbons are ~45% and ~30%, respectively. The development of a new type of catalysts with higher selectivity to middle-distillate products is a challenging research target.[24−26]

It is known that the combination of an acid catalyst, typically a zeolite, with a conventional FT catalyst or an FT active metal into a bifunctional catalyst system may increase the selectivity to gasoline-range hydrocarbons.[27,28] Over such a bifunctional catalyst system, the primary linear hydrocarbons formed on the FT active metal may undergo several secondary reactions (e.g., the isomerization of the linear hydrocarbons, the hydrocracking of heavier hydrocarbons, and the oligomerizations of the light olefins) on the acid site. In a bifunctional catalyst system, the acidic zeolite can be packed in a separate reactor or a separate layer downstream of the FT catalyst[27−29] and can also be mixed with the conventional FT catalyst to form a hybrid catalyst.[27,28,30−32]

To further improve the efficiency of the bifunctional hybrid catalyst, Tsubaki and co-workers[33−36] developed an intriguing

Received: December 19, 2011
Revised: February 8, 2012
Published: February 8, 2012

   dx.doi.org/10.1021/cs200670j | ACS Catal. 2012, 2, 441–449

core−shell structured catalyst system containing a conventional FT catalyst (e.g., Co/SiO_2 or Co/Al_2O_3) as the core and a zeolite membrane as the shell, completely suppressing the formation of C_{12}^+ hydrocarbons. However, the selectivity of CH_4 over these bifunctional catalyst systems is usually high, exceeding 13% in most cases. This is believed to arise from the slow transportation of the products inside the long micropores of zeolites, where the acid sites are located, and the strong acidity of the H-form zeolites. The high selectivities to CH_4 and light (C_2−C_4) alkanes resulting from the overcracking are highly undesirable for FT synthesis.

It is expected that the use of a mesoporous zeolite to replace the conventional microporous zeolite may avoid the overcracking because of the improved mass transport, decreasing the selectivities to CH_4 and C_2−C_4 light alkanes. However, there has been no report on the utilization of mesoporous zeolites for FT synthesis before our work. In a recent communication,[37] we have demonstrated for the first time that a mesoporous ZSM-5-supported Ru catalyst can catalyze the conversion of syngas to C_5−C_{11} hydrocarbons with a very high selectivity (∼80%). H-beta is also efficient for secondary reactions when it is combined with a conventional FT catalyst.[35,36] Studies on the mesoporous beta zeolite are quite limited as compared with the mesoporous ZSM-5 zeolite.[1−10,17,38] Here, we report our detailed studies on the characterizations of the mesoporous beta (meso-beta) zeolite prepared by desilication of H-beta in alkaline medium and the utilization of the meso-beta as the support of Ru catalysts for Fischer−Tropsch synthesis. We have selected Ru as the active metal for FT synthesis in the present work. Despite the higher price of Ru as compared with Co and Fe, Ru-based catalysts are suitable for fundamental research to obtain clear-cut information about the effect of the support because Ru precursors can be easily reduced to Ru^0 and the size of Ru^0 particles can be controlled facilely over different supports. The effects of the mesoporosity and the acidity of the meso-beta on catalytic performances, particularly the product selectivity, for FT synthesis will be discussed to gain insights into the key to the rational design of new FT catalysts with controlled product selectivities.

2. EXPERIMENTAL SECTION

2.1. Catalyst Preparation. H-beta zeolite with a Si/Al ratio of 27 was purchased from Nankai University Catalyst Co. The meso-beta was prepared by treating the H-beta using NaOH aqueous solutions. Typically, H-beta powders (4.0 g) were added into NaOH aqueous solutions (100 mL) with different concentrations in a range of 0.05−0.7 mol dm^{-3} (M), then the suspension was heated to 343 K and stirred at 343 K for 1 h. After being cooled to room temperature, the solid was recovered by filtration, followed by washing thoroughly with deionized water. The recovered solid sample was dried at 373 K for 8 h and calcined in air at 573 K for 3 h. The sample thus obtained is denoted as meso-beta-*x* M, where *x* is the concentration of NaOH. Our inductively coupled plasma mass spectrometry (ICP-MS) analysis suggested that Na^+ ions were exchanged into the cationic sites in the meso-beta. Thus, the meso-beta-*x*M samples were further exchanged into their NH_4^+ forms by adding the meso-beta-*x*M powders into NH_4NO_3 aqueous solution (1.0 M). After the ion-exchanging, the solid product was obtained by filtration, followed by washing, drying, and calcination at 823 K for 6 h. The obtained sample was denoted as H-meso-beta-*x* M, where *x* is the concentration of NaOH used for H-beta treatment.

The supported Ru catalysts were prepared by an impregnation method. Briefly, the meso-beta-*x* M or H-meso-beta-*x* M sample was added into a $RuCl_3$ aqueous solution, and the suspension was stirred for 8 h, followed by resting for 15 h. After evaporation to dryness at 343 K, the solid product was further dried at 323 K in vacuum overnight, followed by calcination in air at 573 K for 3 h. The catalyst was finally reduced in H_2 gas flow at 573 K for 3 h. The loading of Ru in each catalyst was fixed at 3.0 wt %.

2.2. Catalyst Characterization. ICP-MS analyses were performed on an Agilent ICP-MS 4500 instrument. X-ray diffraction (XRD) measurements were carried out on a Panalytical X'pert Pro Super X-ray diffractometer with Cu K_α radiation (40 kV and 30 mA). Argon physisorption at 87 K was performed with a Micromeritics ASAP 2010 M instrument. The sample was pretreated at 573 K in vacuum for 3 h prior to Ar adsorption. The surface area was calculated using the Brunauer−Emmett−Teller (BET) method in the pressure range of P/P_0 = 0.05−0.3. The pore size distribution in the mesoporous region was determined by the Barrett−Joyner−Halenda (BJH) method,[39] and that in the microporous region was evaluated by the Horváth−Kawazoe (HK) method.[40] The microporous volume was estimated by the *t*-plot method.[41] Transmission electron microscopy (TEM) measurements were performed on a Phillips Analytical FEI Tecnai 30 electron microscope operated at an acceleration voltage of 300 kV. Samples for TEM measurements were suspended in ethanol and dispersed ultrasonically. Drops of suspensions were applied on a copper grid coated with carbon.

NH_3-temperature-programmed desorption (NH_3-TPD) measurements were performed using a Micromeritics AutoChem II 2920 instrument. Typically, the sample was pretreated in a quartz reactor with a gas flow containing O_2 and He at 823 K for 1 h, followed by purging with high-purity He. The adsorption of NH_3 was performed at 373 K in an NH_3−He mixture (10 vol % NH_3) for 1 h, and the remaining or weakly adsorbed NH_3 was purged by high-purity He at the same temperature. TPD was performed in He flow by raising the temperature to 1000 K at a rate of 10 K min^{-1}. The desorbed NH_3 was detected using a mass spectrometer by monitoring the signal with m/e = 16. Fourier transform infrared (FT-IR) studies of adsorbed pyridine were performed with a Nicolet 6700 instrument equipped with an MCT detector. The sample was pressed into a self-supported wafer and placed in an in situ IR cell. After pretreatment under vacuum at 673 K for 30 min, the sample was cooled to 473 K, then pyridine was adsorbed at 473 K on the sample for a sufficient time. FT-IR spectra were recorded after gaseous or weakly adsorbed pyridine molecules were removed by evacuation at 473 K.

H_2-temperature-programmed reduction (H_2-TPR) measurements were performed on a Micromeritics AutoChem II 2920 instrument. After the pretreatment of the sample in a quartz reactor with a gas flow containing O_2 and He at 823 K for 1 h, followed by the purge with high-purity He, a H_2−Ar (5 vol % H_2) mixture was introduced into the reactor at 303 K, and the temperature was raised to 1173 K at a rate of 10 K min^{-1}. The consumption of H_2 was monitored by a thermal conductivity detector. Ru dispersions were measured by a H_2−O_2 titration method using a Micromeritics ASAP2010C instrument with the procedures reported in the literature.[42]

dx.doi.org/10.1021/cs200670j | ACS Catal. 2012, 2, 441−449

2.3. Catalytic Reaction. FT synthesis was performed on a fixed-bed, high-pressure, stainless-steel reactor. The catalyst loaded in the reactor with an inner diameter of 7 mm was pretreated in H_2 gas flow (60 mL min^{-1}) at 573 K prior to reaction. After the reactor was cooled to 353 K, a syngas with a H_2/CO ratio of 1/1 was introduced into the reactor. The H_2/CO ratio of 1 is close to that for syngas derived from coal or biomass.[43] The pressure of the syngas was typically regulated to 2.0 MPa. Argon, at a concentration of 4% in the syngas, was used as an internal standard for the calculation of CO conversion. The reaction was started by raising the temperature to the desired reaction temperature. We selected a relatively higher reaction temperature (533 K) in our work because the hydrocracking of heavier hydrocarbons was favored at such a higher temperature. The products were analyzed by gas chromatography. The selectivity was calculated on a carbon basis. Carbon balances were all better than 90%, and catalytic performances typically after 12 h of reaction were used for discussion.

3. RESULTS AND DISCUSSION

3.1. Characterizations of Mesoporous Beta Zeolites. Only a few papers have been devoted to studying the mesoporous beta zeolite prepared by the alkaline-treatment method,[38] although there exist many reports on the alkaline-treated hierarchical ZSM-5.[3−5,7,8] The XRD patterns for our meso-beta samples prepared by treating H-beta with different concentrations of NaOH aqueous solutions at 343 K are shown in Figure 1. The comparison of the XRD patterns of both

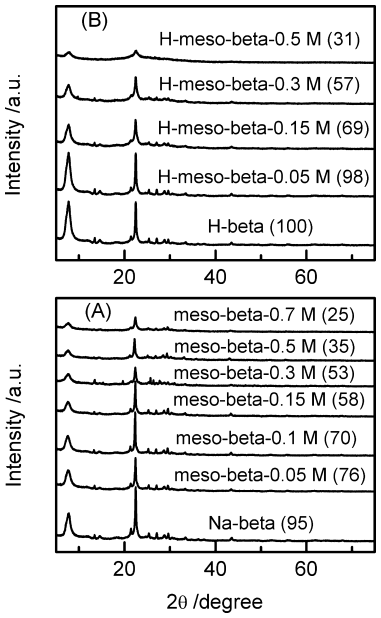

Figure 1. XRD patterns for the meso-beta (A) and the H-meso-beta (B) series of samples along with the parents Na-beta and H-beta zeolites. The number in the parentheses after each sample denotes the relative crystallinity.

meso-beta-*x* M (Figure 1A) and H-meso-beta-*x* M (Figure 1B) series of samples with those of the parent Na-beta and H-beta zeolites confirmed that the crystalline structure of beta zeolite was sustained for both series of samples prepared with suitable concentrations of NaOH. When the concentration of NaOH exceeded 0.15 M, the intensities of the two diffraction peaks at 2θ of 7.7° and 22.4°, which are characteristic of the crystalline beta zeolite, decreased significantly, implying a partial collapse of the crystalline structure under the treatment with higher concentrations of NaOH. We have estimated the relative crystallinity by comparing the areas of diffraction peaks at 2θ of 7.7° and 22.4° among different samples.[44] H-beta zeolite was used as a standard for estimation. The values of relative crystallinity listed in Figure 1 further show the significant decrease in the crystallinity as the concentration of NaOH exceeds 0.15 M. Groen et al.[38] found the damage in the crystalline structure of beta zeolite at higher temperatures (≥338 K) at a fixed concentration of NaOH (0.2 M).

The porous properties of the samples were studied by Ar physisorption at 87 K. Figure 2 shows the adsorption−

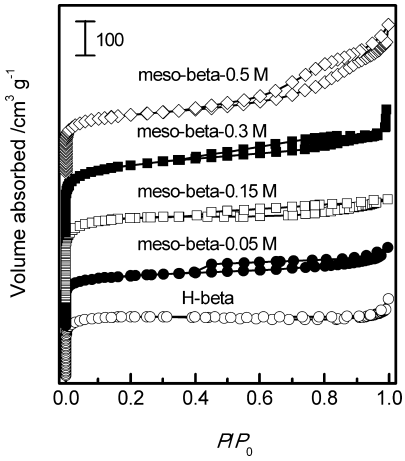

Figure 2. Argon adsorption−desorption isotherms for the meso-beta samples as well as H-beta.

desorption isotherms of meso-beta samples together with H-beta zeolite. The H-beta exhibits the type I isotherm, which is typical of microporous zeolites. The pore size distribution for this sample in the microporous region evaluated by the HK method showed a maximum at 0.67 nm (Figure 3A), which is typical for the beta zeolite. The treatment of H-beta with NaOH aqueous solutions caused the appearance of a hysteresis loop (Figure 2), indicating the generation of mesopores. According to the analysis by the BJH method, the pore diameter in the mesoporous region for the meso-beta sample had a narrow distribution when the concentration of NaOH did not exceed 0.15 M (Figure 3B). For the meso-beta-0.30 M and the meso-beta-0.50 M samples, the pore diameter distribution became relatively broader. The mean diameter of mesopores depended on the concentration of NaOH used for meso-beta preparation; the higher concentration of NaOH resulted in the larger size of the mesopores. The pore diameters and the pore volumes in the microporous and mesoporous regions for meso-beta samples are summarized in Table 1. With the increase in the concentration of NaOH used for the preparation of meso-beta samples, the pore volume in the microporous region (V_{micro}) decreased, and that in the mesoporous region (V_{meso}) increased significantly. The mesoporous surface area, evaluated by the *t*-plot method,[41] also increased significantly with an increase in the concentration of NaOH, up to 0.3 M (Table 1). These results suggest that the alkaline treatment is effective for generating the mesoporosity in the beta zeolite, forming hierarchical mesoporous beta zeolites.

dx.doi.org/10.1021/cs200670j | ACS Catal. 2012, 2, 441−449

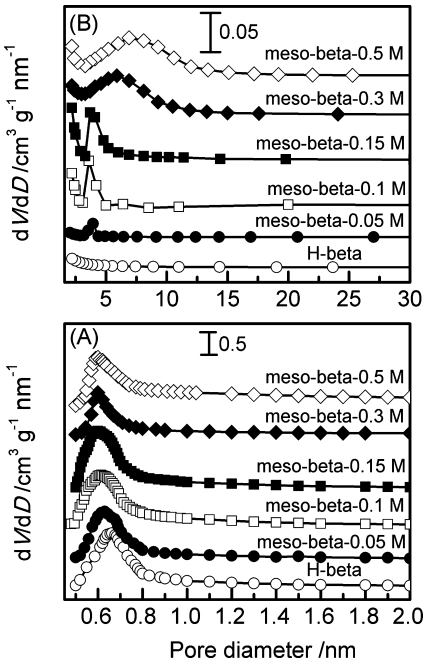

Figure 3. Pore size distributions for the meso-beta samples as well as H-beta: (A) microporous region and (B) mesoporous region.

Table 1. Textural Properties of Mesoporous Beta Zeolites Prepared by Alkaline Treatment

				mean diameter (nm)		pore volume ($cm^3\ g^{-1}$)	
sample	Si/Al ratio[a]	S_{BET}[b] ($m^2\ g^{-1}$)	S_{meso}[c] ($m^2\ g^{-1}$)	D_{micro}[d]	D_{meso}[e]	V_{micro}[f]	V_{meso}[g]
H-beta	27	626	20	0.67		0.21	0.005
meso-beta-0.05 M		599	53	0.63	3.4	0.20	0.033
meso-beta-0.1 M	22	683	121	0.62	4.1	0.17	0.10
meso-beta-0.15 M	21	671	170	0.61	4.4	0.15	0.12
meso-beta-0.3 M	20	642	303	0.60	5.2	0.13	0.32
meso-beta-0.5 M	19	575	213	0.60	7.4	0.12	0.41
meso-beta-0.7 M	17	534	213	0.60	12	0.12	0.51

[a]Si/Al molar ratio measured by ICP-MS. [b]BET surface area. [c]Mesoporous surface area evaluated by the *t*-plot method. [d]Mean pore diameter for micropores estimated by the HK method. [e]Mean pore diameter for mesopores evaluated by the BJH method. [f]Pore volume for micropores evaluated by the *t*-plot method. [g]Pore volume for mesopores evaluated by the BJH method.

TEM was further used to investigate the mesoporosity of our meso-beta samples. Figure 4 presents TEM images of the meso-beta zeolites prepared using different concentrations of NaOH. These TEM images further evidenced the generation of mesopores in the crystalline beta zeolite for the meso-beta samples. The collapse of the zeolite crystal under a higher concentration of NaOH solution (particularly 0.7 M) could also be observed from the TEM images.

It is accepted that the alkaline treatment resulted in the desilication rather dealumination from the framework of zeolites.[3,4,7,8,38] Our ICP-MS measurements reveal that the Si/Al ratio in the meso-beta sample is lower than that in the parent beta zeolite (Table 1), confirming that mainly silicon

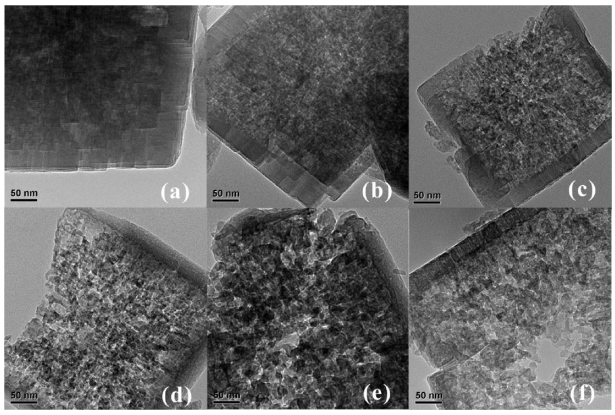

Figure 4. TEM micrographs: (a) H-beta, (b) meso-beta-0.05 M, (c) meso-beta-0.15 M, (d) meso-beta-0.3 M, (e) meso-beta-0.5 M, and (f) meso-beta-0.7 M.

atoms have been removed from the framework of beta zeolite during the treatment by NaOH aqueous solutions.

The acidities of both the meso-beta and the H-meso-beta series of samples were investigated by NH_3-TPD. Figure 5

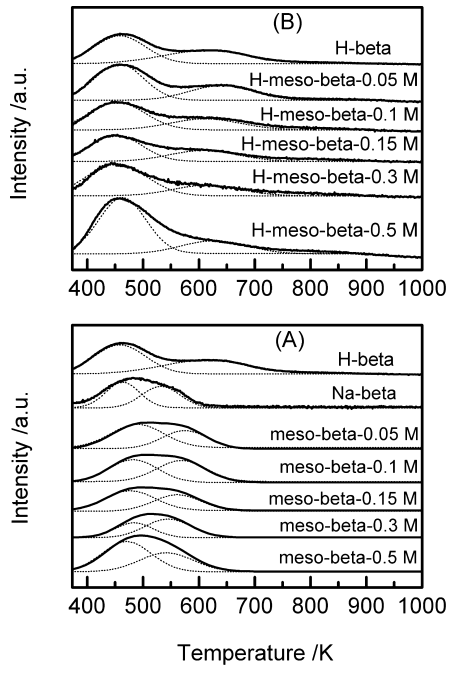

Figure 5. NH_3-TPD profiles for the meso-beta (A) and the H-meso-beta (B) series of samples along with the parents Na-beta and H-beta zeolites.

shows that the parent H-beta exhibits two NH_3 desorption peaks at ~463 and ~630 K. The H-type zeolite usually exhibits two NH_3 desorption peaks; the lower-temperature peak at <500 K may arise from the weakly held (probably hydrogen-bonded) NH_3 molecules, and the higher-temperature peak can be assigned to the desorption of NH_3 molecules chemisorbed on the Brønsted acid sites.[45] A broad peak of NH_3 desorption at a lower temperature was observed for the parent Na-beta. This peak could be deconvolved into two components, and the component at the relatively higher temperature (535 K) can be ascribed to the Lewis acid sites in the Na-beta.

dx.doi.org/10.1021/cs200670j | *ACS Catal.* 2012, 2, 441−449

For our meso-beta series of samples, the ICP-MS analysis clarified that the content of Na was 1.7−2.0 wt %, and the molar ratios of Na/Al in the meso-beta samples were almost unity. This suggests that all the cation-exchanging positions are occupied by the Na^+ ions in the meso-beta samples. Over these samples, in addition to the desorption peak at 460−490 K for the weakly held NH_3 molecules, a NH_3 desorption peak at 550−580 K was observed (Figure 5A), indicating the presence of acidity stronger than the Na-beta. Moreover, the peak temperature, which reflected the strength of the acidity of the meso-beta samples, slightly depended on the concentration of NaOH used for the preparation of these samples; a higher concentration of NaOH shifted the peak to a lower temperature, corresponding to a weaker acidity.

For the H-meso-beta series of samples, our ICP-MS analysis uncovered that the content of Na decreased to ∼0.17 wt % and the molar ratio of Na/Al declined to ∼0.1, indicating that ∼90% of Na^+ cations were exchanged into protons. Figure 5B shows that the H-meso-beta series of samples display a NH_3 desorption peak at >615 K, which is close to that observed for the H-beta and can be ascribed to the Brønsted acid site. This observation indicates that the H-meso-beta series of samples possess strong Brønsted acidity.

To gain further information about the nature of the acidity in these samples, we have performed FT-IR studies of adsorbed pyridine for both meso-beta and H-meso-beta series of samples. Figure 6 shows that the Na-beta zeolite exhibits a sharp IR band

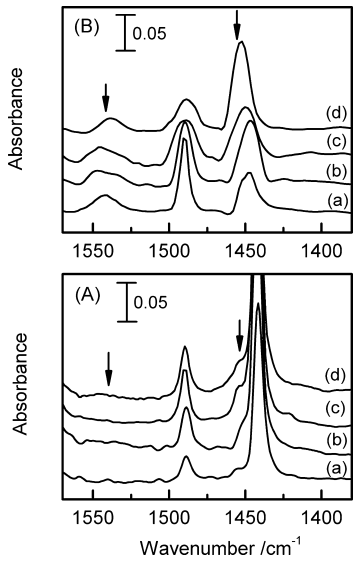

Figure 6. Pyridine-adsorbed FT-IR spectra. (A) Meso-beta series and Na-beta: (a) Na-beta, (b) meso-beta-0.05 M, (c) meso-beta-0.15 M, and (d) meso-beta-0.3 M. (B) H-meso-beta series and H-beta: (a) H-beta, (b) H-meso-beta-0.05 M, (c) H-meso-beta-0.15 M, and (d) H-meso-beta-0.3 M.

at 1442 cm^{-1}, which may arise from the pyridine molecule interacted with weaker Lewis acid sites, such as Na^+. A shoulder band at 1455 cm^{-1}, which could be attributed to the real Lewis acidity, was also observed. As compared with that for Na-beta, the shoulder band at ∼1455 cm^{-1} for the meso-beta samples grew significantly. We speculate that the relatively stronger acid sites on the meso-beta samples observed in NH_3−TPD profiles (Figure 5A) are Lewis acid sites. A similar phenomenon has also been observed for meso-ZSM-5 samples by other groups.[46,47] The nature of these Lewis acid sites is still not clear. It is speculated that these Lewis acid sites may originate from the aluminum species on defective sites after the dissolution of the framework silicon by NaOH treatment.

On the other hand, the H-beta exhibited IR bands at 1542 and 1455 cm^{-1}, attributable to the Brønsted and the Lewis acid sites, respectively.[48] The IR band at 1490 cm^{-1} could stem from both Brønsted acid and Lewis acid sites.[48] Figure 6A suggests that the meso-beta series of samples possess only Lewis acid sites, whereas all the H-meso-beta samples displayed in Figure 6B have both Brønsted and Lewis acid sites. In short, the results from the FT-IR of adsorbed pyridine further confirm that the meso-beta series of samples are dominated by the Lewis acidity, whereas the strong Brønsted acidity exists over the H-meso-beta series of samples.

3.2. Characterizations of Mesoporous Beta Zeolite-Supported Ru Catalysts. Figure 7 shows the H_2-TPR profiles

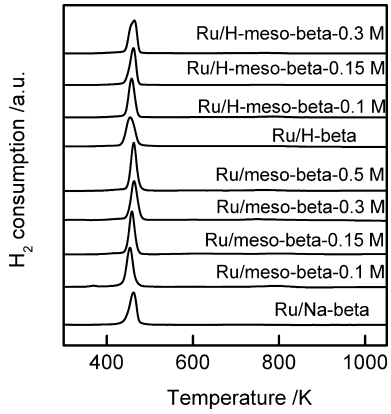

Figure 7. H_2-TPR profiles for the Ru/meso-beta and the Ru/H-meso-beta series of catalysts before H_2 reduction.

for the calcined Ru catalysts loaded on typical meso-beta and H-meso-beta samples before H_2 reduction. All these supported Ru samples displayed a single reduction peak at 455−464 K. The effects of the mesoporosity and the acidity of the support on the reduction behavior were insignificant. We have calculated the degree of reduction of Ru species for each catalyst by quantifying the H_2-TPR result. The degrees of reduction of Ru^{3+} to Ru^0 evaluated from H_2-TPR for the Ru/meso-beta and Ru/H-meso-beta samples are summarized in Table 2. In most cases, the degree of reduction exceeded 85% at 573 K, which has been employed for the reduction of catalyst during the catalyst preparation. Thus, metallic Ru particles are the predominant Ru species over all our catalysts after H_2 reduction.

The mean size of Ru particles over each sample was measured by TEM. Figures 8 and 9 show the typical TEM images for Ru catalysts loaded on typical meso-beta and H-meso-beta samples. The Ru particle size distributions derived by counting ∼200 Ru nanoparticles in these samples are also displayed in Figures 8 and 9. Over most catalysts, the Ru particles were distributed in the range of 4−12 nm, and the maxima are located at 6−8 nm. The mean sizes of Ru nanoparticles over these catalysts were similar, at 5.5−7.7 nm (Table 2). It was reported that Ru particles with a mean size in this range favored FT synthesis.[24,25]

We have also measured the dispersion of Ru nanoparticles over the meso-beta series of samples as well as H-beta by the H_2−O_2 titration method,[42] and the results are summarized in

dx.doi.org/10.1021/cs200670j | ACS Catal. 2012, 2, 441−449

Table 2. Physical Properties of Ru/Meso-Beta and Ru/H-Meso-Beta Catalysts

catalyst	reduction degree at 573 K[a] (%)	mean Ru size[b] (nm)	Ru dispersion[c]	mean Ru size[d] (nm)
Ru/Na-beta	93	7.4	n.d.	n.d.
Ru/meso-beta-0.05 M	92	7.7	0.20	6.6
Ru/meso-beta-0.1 M	90	6.5	0.23	5.7
Ru/meso-beta-0.15 M	85	7.1	0.21	6.3
Ru/meso-beta-0.3 M	84	7.2	0.21	6.3
Ru/meso-beta-0.5 M	90	7.4	0.21	6.3
Ru/H-beta	83	5.5	0.26	5.1
Ru/H-meso-beta-0.05 M	96	n.d.	n.d.	n.d.
Ru/H-meso-beta-0.1 M	90	6.9	n.d.	n.d.
Ru/H-meso-beta-0.15 M	90	7.2	n.d.	n.d.
Ru/H-meso-beta-0.3 M	94	7.3	n.d.	n.d.
Ru/H-meso-beta-0.5 M	86	7.2	n.d.	n.d.

[a]Calculated from H_2-TPR. [b]Evaluated from TEM images. [c]Measured from H_2−O_2 titration. [d]Calculated from the following relationship: particle size (nm) = 1.32/dispersion.[49]

Table 2. The values of Ru dispersions over these catalysts were also quite similar (0.20−0.26). From the values of Ru dispersion, the mean size (d) of Ru particles can be roughly estimated by using the following relationship: d (nm) = 1.32/D, where D is the dispersion of Ru particles.[49] The mean sizes of Ru nanoparticles estimated from the values of Ru dispersions for these catalysts are also listed in Table 2. The mean sizes of Ru obtained from Ru dispersion and those from TEM are consistent with each other.

3.3. Catalytic Behaviors of Mesoporous Beta Zeolite-Supported Ru Catalysts for FT Synthesis. Before discussing the catalytic behaviors of H-meso-beta- or meso-beta-supported Ru catalysts, we have compared the performances of Ru nanoparticles loaded on several types of microporous zeolites as well as on conventional metal oxide supports. As shown in Table 3, the distribution of products was quite wide, and considerable amounts of heavier ($C_{\geq 12}$) hydrocarbons were produced over metal oxide-supported Ru catalysts. The employment of an H-form zeolite as the support decreased the selectivity to $C_{\geq 12}$ and increased that to C_5−C_{11} hydrocarbons, the gasoline-range liquid fuels. The ratio of isoparaffins to n-paraffins in the range of C_5−C_{11} (denoted as C_{iso}/C_n), an indicator of the quality of gasoline, also increased over the zeolite-supported Ru catalysts. This can be attributed to the secondary reactions, including hydrocracking and isomerization of the primary hydrocarbons, over the acid sites in the H-form zeolites.[27,28] However, the selectivity to CH_4 or C_2−C_4 (mainly alkanes) also became significantly higher over these zeolite-supported catalysts as compared with those over the Ru/SiO_2 and Ru/Al_2O_3 catalysts. Among these catalysts, the Ru/H-beta exhibited the highest selectivity to C_5−C_{11} and a relative higher C_{iso}/C_n value.

Although it is still difficult to rationalize the differences in catalytic behaviors among Ru catalysts loaded on different zeolites with different porous structures, it seems that the acidity is a key factor in determining the product distribution. The NH_3-TPD profiles for the microporous zeolites listed in Table 3 are shown in Figure 10. All these zeolites exhibited two NH_3 desorption peaks except for H-mordenite, which displayed a broad peak. As described previously, the higher-temperature peak is attributable to the Brønsted acidity in the H-form zeolite. Thus, the strength of the acidity of these zeolites increases in the following sequence: H-mordenite < H-beta ≈ H-MCM-22 < H-ZSM-5. With increasing the strength of the acidity, the selectivity to C_{12}^+ decreases, but the selectivity to C_5−C_{11} arrives at a maximum over the Ru catalyst loaded on H-beta with a medium strength of acidity. The tendency in Table 3 indicates that the stronger acidity of zeolite may cause overcracking, leading to higher selectivity to lighter (i.e., C_1−C_4) hydrocarbons.

Figure 11 shows the catalytic performances of Ru catalysts loaded on H-meso-beta samples prepared by treating H-beta with different concentrations of NaOH, followed by NH_4^+ exchanging and calcination. The use of H-meso-beta instead of

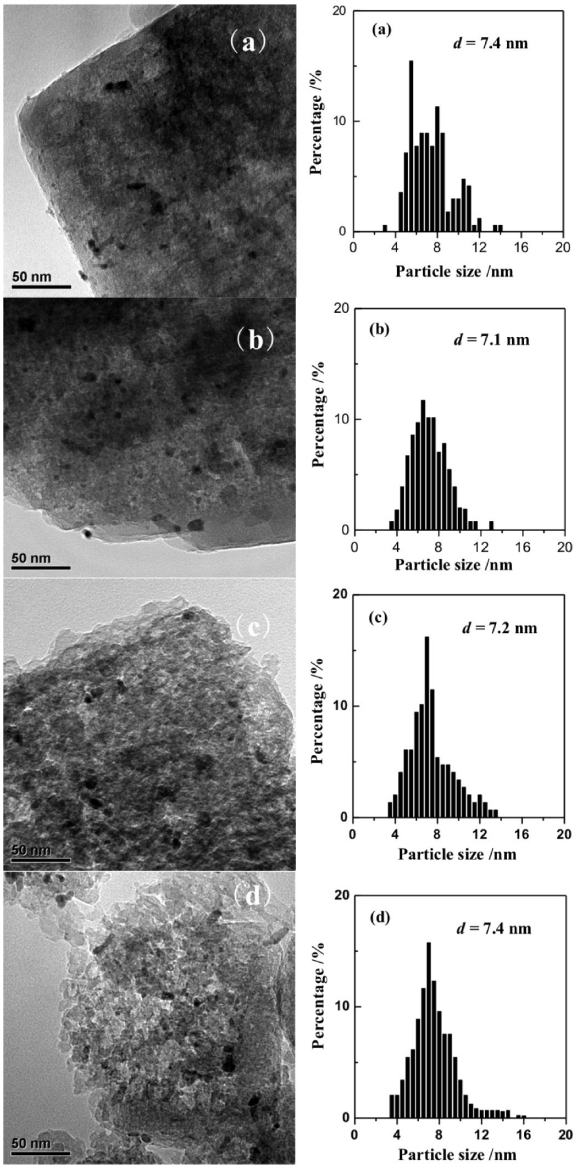

Figure 8. TEM micrographs for the Ru/meso-beta series of catalysts as well as the Ru/Na-beta: (a) Ru/Na-beta, (b) Ru/meso-beta-0.15 M, (c) Ru/meso-beta-0.3 M, and (d) Ru/meso-beta-0.5 M.

dx.doi.org/10.1021/cs200670j | ACS Catal. 2012, 2, 441−449

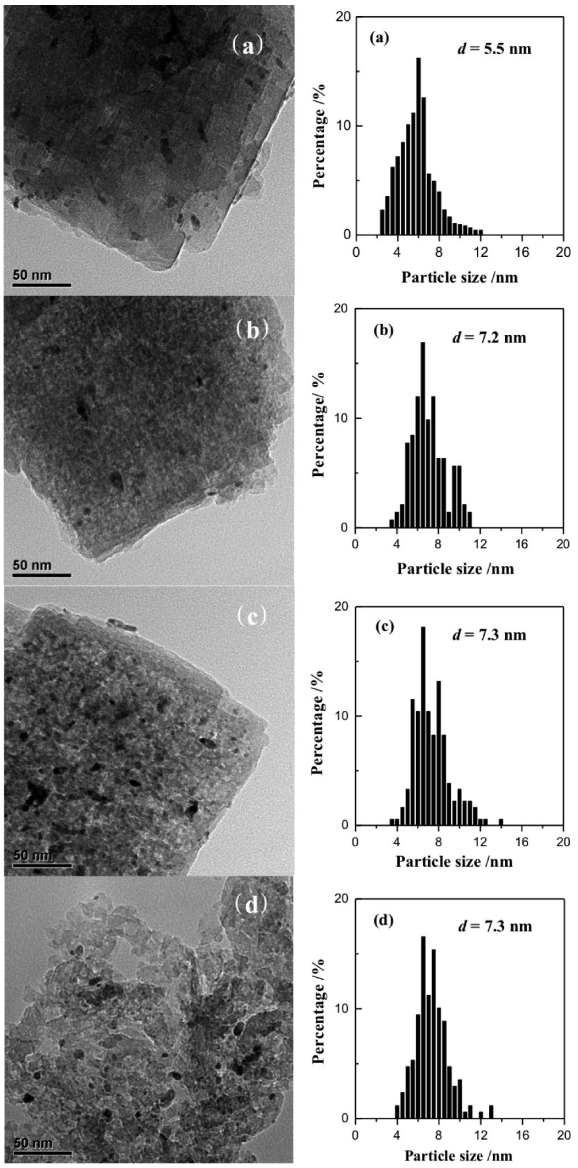

Figure 9. TEM micrographs for the Ru/H-meso-beta series of catalysts as well as the Ru/H-beta: (a) Ru/H-beta, (b) Ru/H-meso-beta-0.15 M, (c) Ru/H-meso-beta-0.2 M, and (d) Ru/H-meso-beta-0.3 M.

H-beta (NaOH concentration = 0 M in Figure 11) as the support of Ru decreased the selectivity of CH_4. For example, the selectivity of CH_4 decreased from 14% over the Ru/H-beta to 11% and 7.9% over the Ru/H-meso-beta-0.1 M and the Ru/H-meso-beta-0.15 M catalysts, respectively. The selectivity to C_{12}^+ also declined when the H-meso-beta-0.1 M and the H-meso-beta-0.15 M were used. A further increase in the concentration of NaOH to 0.3 M increased the selectivity to C_{12}^+ again. Thus, the highest selectivity to C_5–C_{11} hydrocarbons for this series of catalysts was attained over the Ru/H-meso-beta-0.15 M catalyst (67%). CO conversion increased gradually with an increase in the concentration of NaOH used for H-meso-beta preparation (Figure 11B). The C_{iso}/C_n ratio remained at >3 when the concentration of NaOH was kept at ≤0.15 M.

The ratio of olefins to *n*-paraffins in C_5–C_{11} hydrocarbons (denoted as C_{ole}/C_n) is also shown in Figure 11B. The C_{ole}/C_n ratio changed in the range of 0.15–0.41 when the concentration of NaOH changed from 0 to 0.3 M. Thus, isoparaffins are the dominant products over our Ru/H-meso-

Table 3. Catalytic Performances of Ru Loaded on Several Microporous Zeolites as Well as Metal Oxides for FT Synthesis[a]

		hydrocarbon selectivity (%)				
catalyst[b]	CO conv(%)	CH_4	C_{2-4}	C_{5-11}	$C_{\geq 12}$	C_{iso}/C_n[c]
Ru/SiO_2	32	6.8	10	25	57	0.42
Ru/Al_2O_3	40	3.1	6.8	22	68	0.53
Ru/TiO_2	20	14	36	26	25	1.1
Ru/H-mordenite (12)	31	11	18	52	19	1.8
Ru/H-beta (27)	24	14	21	58	6.9	3.3
Ru/H-MCM-22 (30)	22	10	35	54	0	4.1
Ru/H-ZSM-5 (26)	25	15	37	47	0.7	2.7

[a]Reaction conditions: W = 0.5 g, H_2/CO = 1/1, P = 2 MPa, F = 20 cm^3/min, T = 533 K, time on stream = 12 h. [b]Ru loading is 3.0 wt % in each catalyst; the number in the parentheses denotes the Si/Al ratio. [c]The molar ratio of isoparaffins to *n*-paraffins in the range of C_5–C_{11}.

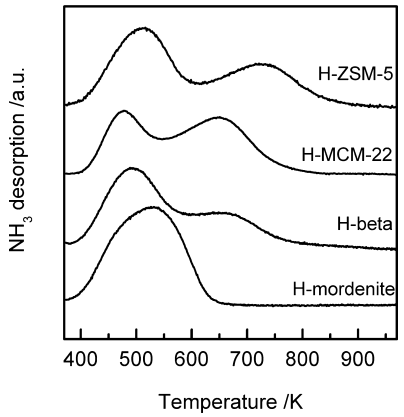

Figure 10. NH_3-TPD profiles for several zeolites.

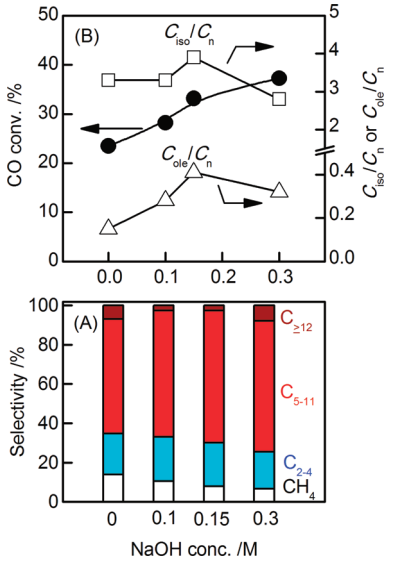

Figure 11. Catalytic performances of the Ru/H-meso-beta catalysts as well as the Ru/H-beta: (A) product selectivity; (B) CO conversion, C_{iso}/C_n, and C_{ole}/C_n. Reaction conditions: W = 0.5 g, H_2/CO = 1/1, P = 2 MPa, F = 20 cm^3/min, T = 533 K, time on stream =12 h.

dx.doi.org/10.1021/cs200670j | ACS Catal. 2012, 2, 441–449

beta catalysts. Our characterizations have clarified that the reduction degree of Ru species and the mean sizes of Ru particles are similar over these catalysts (Table 2). Moreover, the acidities of the H-meso-beta series of samples were also similar and were comparable to the H-beta (Figures 5 and 6). Thus, these results allow us to consider that the differences in catalytic behaviors among the catalysts in Figure 11 mainly result from the difference in the mesoporosity of the support.

We propose that the mesoporosity in the H-meso-beta can enhance the mass transport, contributing to the higher CO conversion and the lower CH_4 selectivity. The presence of mesoporosity can also enhance the accessibility of primary products, that is, the linear hydrocarbons, formed on Ru nanoparticles to the acid sites. In other words, the number of the effective acid sites capable of catalyzing the hydrocracking and isomerization was increased over the catalysts with proper mesoporosity. This resulted in the decrease in the selectivity of C_{12}^+ by using H-meso-beta-0.1 M and H-meso-beta-0.15 M to replace H-beta (Figure 11A). However, when the concentration of NaOH used for preparation of H-meso-beta was too high (≥0.3 M), the partial collapse of the crystalline structure of the zeolite may decrease the number of acid sites (Figure 5B), leading to the lower hydrocracking ability and the higher C_{12}^+ selectivity (Figure 11).

We further performed FT synthesis over the Ru catalysts loaded on the meso-beta series of samples without strong Brønsted acidity. The catalytic behaviors of these catalysts are shown in Figure 12. The Ru/Na-beta catalyst (NaOH concentration =0 M in Figure 12) showed a significantly higher selectivity of C_{12}^+ (22%) than the Ru/H-beta (6.9%, Figure 11). The C_{iso}/C_n ratio was also lower over the Ru/Na-beta catalyst. These are expected to arise from the fact that Na-beta possesses only Lewis acidity (Figures 5 and 6), over which the hydrocracking and isomerization proceed less efficiently. The weaker acidity also led to a relatively lower selectivity of CH_4 (7.2%) over the Ru/Na-beta than that over the Ru/H-beta (14%).

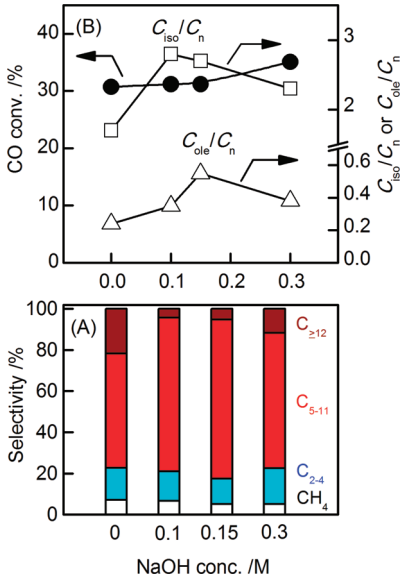

Figure 12. Catalytic performances of the Ru/meso-beta catalysts as well as the Ru/Na-beta: (A) product selectivity; (B) CO conversion, C_{iso}/C_n, and C_{ole}/C_n. Reaction conditions: W = 0.5 g, H_2/CO = 1/1, P = 2 MPa, F = 20 cm^3/min, T = 533 K, time on stream = 12 h.

From Figure 12, it is of significance to find that the use of meso-beta instead of Na-beta as the support could further decrease the selectivity of CH_4. For example, the selectivity of CH_4 over the Ru/meso-beta-0.15 M decreased to 5.2%. This further confirms the role of the mesoporosity in inhibiting the formation of CH_4 by accelerating the mass transport. Furthermore, the selectivity to C_{12}^+ hydrocarbons became considerably lower over the Ru/meso-beta catalysts than that over the Ru/Na-beta catalyst. For example, the C_{12}^+ selectivity decreased from 22% over the Ru/Na-beta to 4.3% and 5.1% over the Ru/meso-beta-0.1 M and Ru/meso-beta-0.15 M catalysts, respectively. We speculate that, in addition to the mesoporosity that increases the accessibility of the primary product to the acid sites in meso-beta, that is, the increase in the number of effective acid sites for hydrocracking and isomerization, the stronger acidity of the meso-beta as compared with Na-beta (Figure 5) may also contribute to the enhanced hydrocracking ability of the Ru/meso-beta catalysts. As a result, Ru/meso-beta-0.10 M and Ru/meso-beta-0.15 M catalysts displayed better C_5−C_{11} selectivities (75% and 77%), which were much higher than the maximum C_5−C_{11} selectivity expected from ASF distribution (~45%).

The C_{iso}/C_n ratios over these two catalysts (2.8 and 2.7) were also higher than those over the Ru/Na-beta (1.7) and the Ru/meso-beta-0.3 M (2.3) catalysts. The C_{ole}/C_n ratios over the Ru/meso-beta-0.10 M and the Ru/meso-beta-0.15 M were 0.35 and 0.55. Although the C_{ole}/C_n ratios over the Ru/meso-beta catalysts became higher than that over the Ru/Na-beta (0.24), isoparaffins were the main products over the former catalysts. The fractions of olefins over our Ru/H-meso-beta and Ru/meso-beta catalysts are comparable with those over the core−shell structured bifunctional FT catalysts reported previously, which contained a conventional FT catalyst as the core and a zeolite membrane as the shell.[35]

4. CONCLUSIONS

Two series of mesoporous beta zeolites (i.e., meso-beta and H-meso-beta) were successfully prepared by a simple alkaline post-treatment method. The size and volume of mesopores depended on the concentration of NaOH used for post-treatment. The higher concentration of NaOH led to the generation of mesopores with larger sizes and volumes, but the crystalline structure of beta zeolite underwent partial collapse under treatment in NaOH aqueous solutions with higher concentrations. The meso-beta series of samples obtained without further ion-exchanging contained Na^+ cations in the ion-exchanging positions and were dominated by Lewis acidity, whereas the H-meso-beta series of samples after ion-exchanging with NH_4^+ followed by calcination displayed Brønsted acidity similar to that of H-beta. Ru/H-beta showed relatively higher selectivity to C_5−C_{11} hydrocarbons as compared with Ru/H-mordenite, Ru/H-MCM-22, and Ru/H-ZSM-5, possibly because of the medium-strength Brønsted acidity of H-beta zeolite. The use of H-meso-beta prepared using a proper concentration of NaOH (≤0.15 M) instead of H-beta as the support of Ru decreased the selectivities to both CH_4 and heavier hydrocarbons (C_{12}^+) and increased that to C_5−C_{11} hydrocarbons. CO conversion was also increased, and the ratio of isoparaffins to *n*-paraffins kept at >3. Ru/Na-beta exhibited a lower selectivity of CH_4 but a higher selectivity of C_{12}^+ hydrocarbons because Na-beta possessed only Lewis acidity. The use of meso-beta dominated by Lewis acidity as the support could not only further decrease the selectivity of CH_4

dx.doi.org/10.1021/cs200670j | ACS Catal. 2012, 2, 441−449

but also significantly reduce the C_{12}^+ selectivity. A 77% selectivity to C_5−C_{11} hydrocarbons with a ratio of isoparaffins to *n*-paraffins being 2.7 could be attained over Ru/meso-beta-0.15 M catalyst. The mesoporosity and the unique acidity of the meso-beta sample are proposed to contribute to the selective hydrocracking of heavier hydrocarbons to C_5−C_{11} hydrocarbons.

AUTHOR INFORMATION

Corresponding Author

*Phone: +86-592-2186156. Fax: +86-592-2183047. E-mail: (Y.W.) wangye@xmu.edu.cn, (Q.Z.) zhangqh@xmu.edu.cn.

Notes

The authors declare no competing financial interest.

ACKNOWLEDGMENTS

This work was supported by the National Basic Program of China (Nos. 2010CB732303), Natural Science Foundation of China (Nos. 21173174, 21033006, 21161130522, and 209230049), the Key Scientific Project of Fujian Province (2009HZ0002-1), and the Program for Changjiang Scholars and Innovative Research Team in University (No. IRT1036).

REFERENCES

(1) van Donk, S.; Janssen, A. H.; Bitter, J. H.; de Jong, K. P. *Catal. Rev.* **2003**, *45*, 297−319.
(2) Hartmann, M. *Angew. Chem., Int. Ed.* **2004**, *43*, 5880−5882.
(3) Groen, J. C.; Moulijn, J. A.; Pérez-Ramírez, J. *J. Mater. Chem.* **2006**, *16*, 2121−2131.
(4) Pérez-Ramírez, J.; Christensen, C. H.; Egeblad, K.; Christensen, C. H.; Groen, J. C. *Chem. Soc. Rev.* **2008**, *37*, 2530−25342.
(5) Schmidt, W. *ChemCatChem* **2009**, *1*, 53−67.
(6) Meng, X.; Nawaz, F.; Xiao, F. S. *Nano Today* **2009**, *4*, 292−301.
(7) Chal, R.; Gérardin, C.; Bulut, M.; van Donk, S. *ChemCatChem* **2011**, *3*, 67−81.
(8) Verboekend, D.; Pérez-Ramírez, J. *Catal. Sci. Technol.* **2011**, *1*, 879−890.
(9) Chen, H.; Wydra, J.; Zhang, X.; Lee, P. S.; Wang, Z.; Fan, W.; Tsapatsis, M. *J. Am. Chem. Soc.* **2011**, *133*, 12390−12393.
(10) Zhu, K.; Sun, J.; Liu, J.; Wang, L.; Wan, H.; Hu, J.; Wang, Y.; Peden, C. H. F.; Nie, Z. *ACS Catal.* **2011**, *1*, 682−690.
(11) Christensen, C. H.; Johannsen, K.; Schmidt, I.; Christensen, C. H. *J. Am. Chem. Soc.* **2003**, *125*, 13370−13371.
(12) Groen, J. C.; Sano, T.; Moulijn, J. A.; Pérez-Ramírez, J. *J. Catal.* **2007**, *251*, 21−27.
(13) van Laak, A. N. C.; Sagala, S. L.; Zečević, J.; Friedrich, H.; de Jong, P. E.; de Jong, K. P. *J. Catal.* **2010**, *276*, 170−180.
(14) de Jong, K. P.; Zečević, J.; Friedrich, H.; de Jong, P. E.; Bulut, M.; van Donk, S.; Kenmogne, R.; Finiels, A.; Hulea, V.; Fajula, F. *Angew. Chem., Int. Ed.* **2010**, *49*, 10074−10078.
(15) Qin, Z.; Shen, B.; Gao, X.; Lin, F.; Wang, B.; Xu, C. *J. Catal.* **2011**, *278*, 266−275.
(16) Zhou, J.; Hua, Z.; Liu, Z.; Wu, W.; Zhu, Y.; Shi, J. *ACS Catal.* **2011**, *1*, 287−291.
(17) Tang, T.; Yin, C.; Wang, L.; Ji, Y.; Xiao, F. S. *J. Catal.* **2007**, *249*, 111−115.
(18) Kim, J.; Choi, M.; Ryoo, R. *J. Catal.* **2010**, *269*, 219−228.
(19) Khodakov, A. Y.; Chu, W.; Fongarland, P. *Chem. Rev.* **2007**, *107*, 1692−1774.
(20) Davis, B. H. *Ind. Eng. Chem. Res.* **2007**, *46*, 8938−8945.
(21) Hao, X.; Dong, G.; Yang, Y.; Xu, Y.; Li, Y. *Chem. Eng. Technol.* **2007**, *30*, 1157−1165.
(22) van Steen, E.; Claeys, M. *Chem. Eng. Technol.* **2008**, *31*, 655−666.
(23) de Smit, E.; Weckhuysen, B. M. *Chem. Soc. Rev.* **2008**, *37*, 2758−2781.
(24) Zhang, Q.; Kang, J.; Wang, Y. *ChemCatChem* **2010**, *2*, 1030−1058.
(25) Kang, J.; Zhang, S.; Zhang, Q.; Wang, Y. *Angew. Chem., Int. Ed.* **2009**, *48*, 2565−2568.
(26) Yu, G.; Sun, B.; Pei, Y.; Xie, S.; Yan, S.; Qiao, M.; Fan, K.; Zhang, X.; Zong, B. *J. Am. Chem. Soc.* **2010**, *132*, 935−937.
(27) Martínez, A.; Prieto, G. *Top. Catal.* **2009**, *52*, 75−90.
(28) Sun, B.; Qiao, M.; Fan, K.; Ulrich, J.; Tao, F. *ChemCatChem* **2011**, *3*, 542−550.
(29) Botes, F. G.; Böhringer, W. *Appl. Catal. A* **2004**, *267*, 217−225.
(30) Tsubaki, N.; Yoneyama, Y.; Michiki, K.; Fujimoto, K. *Catal. Commun.* **2003**, *4*, 108−111.
(31) Zhao, T.; Chang, J.; Yoneyama, Y.; Tsubaki, N. *Ind. Eng. Chem. Res.* **2005**, *44*, 769−775.
(32) Martínez, A.; Rollán, J.; Arribas, M. A.; Cerqueira, H. S.; Aguiar, E. F. S. *J. Catal.* **2007**, *249*, 162−173.
(33) He, J.; Yoneyama, Y.; Xu, B.; Nishiyama, N.; Tsubaki, N. *Langmuir* **2005**, *21*, 1699−1702.
(34) He, J.; Liu, Z.; Yoneyama, Y.; Nishiyama, N.; Tusbaki, N. *Chem.—Eur. J.* **2006**, *12*, 8296−8304.
(35) Bao, J.; He, J.; Zhang, Y.; Yoneyama, Y.; Tsubaki, N. *Angew. Chem., Int. Ed.* **2008**, *47*, 353−356.
(36) Li, X.; He, J.; Meng, M.; Yoneyama, Y.; Tsubaki, N. *J. Catal.* **2009**, *265*, 26−34.
(37) Kang, J.; Cheng, K.; Zhang, L.; Zhang, Q.; Ding, J.; Hua, W.; Lou, Y.; Zhai, Q.; Wang, Y. *Angew. Chem., Int. Ed.* **2011**, *50*, 5200−5203.
(38) Groen, J. C.; Abelló, S.; Villaescusa, L. A.; Pérez-Ramírez, J. *Microporous Mesoporous Mater.* **2008**, *114*, 93−102.
(39) Barrett, E. P.; Joyner, L. S.; Halenda, P. P. *J. Am. Chem. Soc.* **1951**, *73*, 373−380.
(40) Horváth, G.; Kawazoe, K. *J. Chem. Eng. Jpn.* **1983**, *16*, 470−475.
(41) Cranston, R.; Inkley, F. *Adv. Catal.* **1957**, *9*, 143−154.
(42) Taylor, K. C. *J. Catal.* **1975**, *38*, 299−306.
(43) Tomishige, K.; Asadullah, M.; Kunimori, K. *Catal. Today* **2004**, *89*, 389−403.
(44) Camblor, M. A.; Corma, A.; Valencia, S. *Microporous Mesoporous Mater.* **1998**, *25*, 59−74.
(45) Katada, N.; Igi, H.; Kim, J. H.; Niwa, M. *J. Phys. Chem. B* **1997**, *101*, 5969−5977.
(46) Fernandez, C.; Stan, I.; Gilson, J. P.; Thomas, K.; Vicente, A.; Bonilla, A.; Pérez-Ramírez, J. *Chem.—Eur. J.* **2010**, *16*, 6224−6233.
(47) Holm, M. S.; Svelle, S.; Joensen, F.; Beato, P.; Christensen, C. H.; Bordiga, S.; Bjørgen, M. *Appl. Catal. A* **2009**, *356*, 23−30.
(48) Koo, J. B.; Jiang, N.; Saravanamurugan, S.; Bejblová, M.; Musilová, Z.; Čejka, J.; Park, S. E. *J. Catal.* **2010**, *276*, 327−334.
(49) Álvarez-Rodríguez, J.; Guerrero-Ruiz, A.; Rodríguez-Ramos, I.; Arcoya-Martín, A. *Catal. Today* **2005**, *107*−*108*, 302−309.